



## Transport of salt and suspended sediments in a curving channel of a coastal plain estuary: Satilla River, GA

Jackson O. Blanton<sup>a,\*</sup>, Harvey Seim<sup>a,1</sup>, Clark Alexander<sup>a</sup>, Julie Amft<sup>a</sup>, Gail Kineke<sup>b</sup>

<sup>a</sup>*Skidaway Institute of Oceanography, 10 Ocean Science Circle, Savannah, GA 31411, USA*

<sup>b</sup>*Department of Geology and Geophysics, Boston College, Chestnut Hill, MA 02167, USA*

Received 28 May 2002; accepted 22 January 2003

### Abstract

This study describes the transport of salt and suspended sediment in a curving reach of a shallow mesotidal coastal plain estuary. Circulation data revealed a subtidal upstream bottom flow during neap tide, indicating the presence of a gravitational circulation mode throughout the channel. During spring tide, landward bottom flow weakened considerably at the upstream end of the channel and changed to seaward in the middle and downstream areas of the reach, suggesting the importance of tidal pumping. Salt flux near-bottom was landward at both ends of the channel during neap tide. At spring, however, the salt flux diverged along the bottom of the thalweg suggesting that tidal pumping caused a transfer of salt vertically and laterally into the intertidal zone. Thus, landward flux of salt is maintained even in the presence of subtidal seaward flow along the bottom at the downstream end of the channel.

Landward bottom stress is greater than seaward stress, preferentially transporting suspended sediments upstream. Compared with salt, however, the weight of the suspended sediments causes less upward transfer of sediments into the intertidal zone. Flood flow carried more suspended sediments landward at the upstream end compared with the downstream end. We speculate that secondary flow in the curving channel picks up increasing amounts of suspended sediments along the sides during flood and adds them to the axial flow in the thalweg. Since the landward flow along the bottom of the thalweg weakens and even reverses during spring tide, there appears to be a complex re-circulation system for sediments re-suspended in curving channels that complicates the picture of a net transport of sediments landward.

© 2003 Elsevier Ltd. All rights reserved.

*Keywords:* estuaries; Satilla River; salt transport; sediment transport; secondary circulation; estuarine dynamics; USA; Georgia

### 1. Introduction

The Satilla River drains a watershed of 9140 km<sup>2</sup> in the coastal plain of Georgia. An extensive salt marsh fringes the estuarine system and the intertidal region accounts for more than 70% of the total area. The estuary experiences 1–1.5 m semi-diurnal tidal amplitude, which produces depth-averaged tidal currents up to 1 m s<sup>-1</sup> amplitude. The main channel, seldom greater than 10-m depth, follows a sinuous path that extends more than 50 km inland. In the lower 25 km of the estuary the

main trunk is relatively broad (O(1 km)) and has primary and secondary channels. Freshwater inflow to the estuary is small, averaging 70 m<sup>3</sup> s<sup>-1</sup>, but occasionally rises in excess of 300 m<sup>3</sup> s<sup>-1</sup> during rainy periods and falls to nearly zero during severe droughts. Vertical stratification is typically weak at spring tides (2 kg m<sup>-3</sup> vertical density change) and stronger during neap tides (5 kg m<sup>-3</sup> vertical change) and is dominated by salinity variations.

The Satilla has a heterogeneous source of sediments along the fringes of the salt marshes. It has one of the largest tidal marshes and tidal prism of any estuary along the southeastern coast of the US (Oertel & Dunstan, 1981), providing a strong source of suspended sediments. Weakly consolidated mud aprons are found along the flanks of the main channel. Presumably, the

<sup>1</sup> Now at University of North Carolina, Chapel Hill.

\* Corresponding author.

E-mail address: [jack@skio.peachnet.edu](mailto:jack@skio.peachnet.edu) (J.O. Blanton).

degree of consolidation increases as turbulent kinetic energy in the tidal current decreases from spring to neap (Allen, Salomon, Bassoulet, Penhout, & DeGranpre, 1980). While we cannot verify neap to spring variations in consolidation, we show observations that are consistent with such variations.

Sources of sediment to the estuary are varied: import from the ocean, retention of riverine material, and recycling of salt-marsh and tidal flat sediments by erosion. Each of these sources seems to be locally important and contributes to the spatial heterogeneity of the estuarine system. Additional complications arise because the river channel is effectively divided into compartments by large sand shoals near the mouth, at Bailey Cut, and at the east end of Crows Harbor Reach (Fig. 1). These compartments may each have their own internal sediment sources that are remobilized and redistributed by tidal energy. Hence, a classical estuarine turbidity maximum is unlikely to form, or if formed, be maintained for any significant length of time in any one region along the axis.

Large concentrations of suspended sediments are mobilized between slack-water periods (Blanton, Alexander, Alber, & Kineke, 1999). Fast-settling particles with high concentrations can reach the bottom within an hour or so, thus spending most of the time near or on the bottom. At lower concentrations, the particles are slow-settling and cannot reach the bottom within a slack-water interval except in shallow intertidal areas where the strength of the current is considerably reduced. Large intertidal areas are found within the small shallow tidal creeks feeding large expanses of salt marsh and presumably accounts for the presence of very fine-grained sediments on the beds of these environments (Postma,

1961). We speculated, based on levels of organic carbon (Blanton et al., 1999), that much of the suspended sediment load is lifted off fringing intertidal salt-marshes and mud aprons at the marsh edge, and becomes entrained in the flow in the deeper part of the channel where it is moved back and forth by tidal currents.

Large billows of mud resuspended from the bottom are often observed at the surface during the tidal cycle (Blanton et al., 1999). These billows have a horizontal scale of about 1 m. Near-bottom concentrations can exceed  $1 \text{ g l}^{-1}$  and reach as high as  $8 \text{ g l}^{-1}$ . The most dramatic suspended sediment concentration (SSC) profiles occur within the first 2 h of flood when mud layers about 1–2 m thick over the bottom have concentrations between 2 and  $4 \text{ g l}^{-1}$ . Sediment fall velocities span three orders of magnitude from  $0.001$  to  $1 \text{ mm s}^{-1}$  in the main channel.

The conventional model of estuarine sediment transport is that the estuarine circulation drives a landward sediment flux where it meets seaward flux carried by a river. The exact meeting position is governed by an interplay between gravitational circulation, tidal pumping, and sediment dynamics (Dyer, 1997). Net seaward flux of sediment is driven by large discharge events that overwhelm the estuarine circulation and result in episodic export of large quantities of sediment to the ocean (Geyer, Woodruff, & Traykovski, 2001).

This article focuses on the transport of salinity and suspended sediments in a curving channel of the Satilla River estuary (Fig. 2). We focus on the channel's spatial gradients of velocity, salinity, and SSC and how they change in response to the spring–neap cycle. A month-long data set is used to describe the circulation and flux of salt and sediment over a limited reach of the Satilla

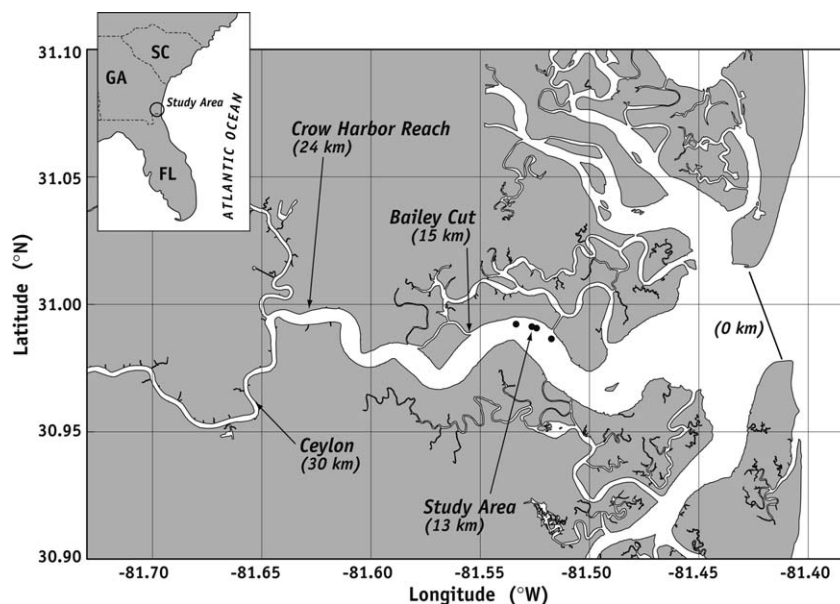


Fig. 1. Location of study.

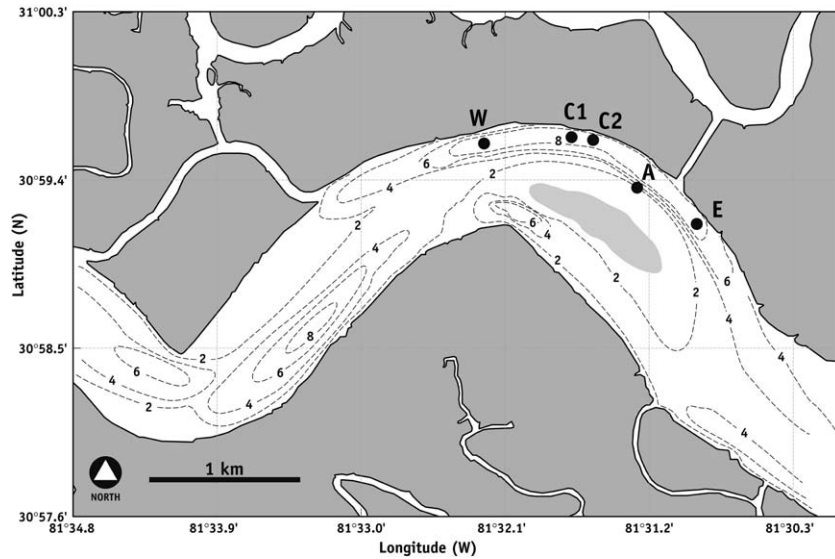


Fig. 2. Map of mooring domain.

River estuary that includes a sharp channel bend. Low-frequency changes in salinity and currents are described during a period of steadily decreasing river discharge that represents a period of non-export of sediments. A detailed description of tidal flow and its effect on salinity and SSC is presented. The article ends with a discussion of the role of subtidal flow regime in the distribution of suspended sediments.

2. Data sources

2.1. Mooring field

A set of moorings were installed in the study area (Fig. 2). Table 1 shows the instruments used in the study domain. The instruments were located in a curved chan-

nel with a radius of curvature of about 2.5 km. One mooring was placed at the western end of the domain (Site W) where the channel had its maximum curvature. Another set of instruments were placed downstream where the channel was still strongly curved (Sites C1 and C2). The easternmost mooring (Site E) was located where the channel is relatively straight. Sites W and E each had an InterOcean S-4 current meter mounted 1 m above bottom (mab) and two SeaBird Electronics SeaCat temperature, conductivity, pressure, and optical backscatterance (OBS) monitors. The SeaCats were placed at 0.06 and 2.5 mab. The SeaCats and S-4s recorded data every 6 min.

A Benthic Acoustic Stress Sensor (BASS) and an RDI 600 kHz broadband acoustic Doppler current profiler (ACDP) were placed between the east and west sites. The ADCP measured velocity at 0.5 m intervals

Table 1  
Instruments and sensors used in the study area ((see Fig. 2); except for BASS, data spanned from 25 March to 27 April 1997)

Station	Sensor depth (mab)	Water depth (m)	Instrument	Parameters measured	Latitude (deg N)	Longitude (deg W)
A		9.6	Anchor Station	C,OBS,P,T,V+	30.9909	81.5197
E	2.50	10.0	SBE-SeaCat	C,OBS,P,T	30.9932	81.5378
E	1.00	10.0	IntOc S4	C,T,V	30.9932	81.5378
E	0.66	10.0	SBE-SeaCat	C,OBS,P,T	30.9932	81.5378
C1		9.5	RDI ADCP	V+	30.9937	81.5270
C2	0.28–1.28	9.6	BASS <sup>a</sup>	V+	30.9928	81.5249
C2	2.50	9.6	SBE-SeaCat	C,T	30.9928	81.5249
C2	0.66	9.6	SBE-SeaCat	C,OBS,P,T	30.9928	81.5249
W	2.50	10.3	SBE-SeaCat	C,OBS,P,T	30.9856	81.5143
W	1.00	10.3	IntOc S4	C,T,V	30.9856	81.5143
W	0.66	10.3	SBE-SeaCat	C,OBS,P,T	30.9856	81.5143

mab, meters above bottom; C, conductivity; OBS, optical backscatterance; P, subsurface pressure; T, water temperature; V, current velocity; V+, current velocity profiles.

<sup>a</sup> End date = 6 April 1997.

beginning at 2.24 mab and extending to within a meter of the free surface. Bin averages of the current profiles were recorded every 12 min. BASS (Williams et al., 1987) measured turbulent velocities at levels of 0.28, 0.66, 0.98, and 1.28 mab and collected 4.5-min bursts of 2 Hz data every 10 min.

SeaBird sensors yielded identical conductivity values to the nearest 100th in mixed tanks of three different salinities, so salinity data are judged to be generally of excellent quality. However, the salinity data of the lower meter at the east site had questionable values from time to time, probably due to clogging by mud. All OBS sensors became fouled after about 16 days of operation. The BASS unit tipped over after 10 days, a period which was enough to span a spring–neap interval.

## 2.2. Ship surveys

Four axial surveys were conducted along the thalweg of the estuary to measure profiles of temperature, salinity, and OBS. The first survey was done before in situ instruments were deployed, the second during a spring tide, the third during the following neap tide and the final after the in situ instruments were retrieved. These surveys monitored the shifting of the axial salinity field over the mooring period.

The ship was anchored for two tidal cycles during the spring and neap tide periods at a location 400 m seaward of Station C2 (Fig. 2). A suspended sediment profiler ('GAFANHOTO') was used during the axial surveys and anchor stations to obtain water column data on water properties, flow conditions, and SSCs. GAFANHOTO (Sternberg, Kineke, & Johnson, 1991) is an open frame tripod with a trapezoidal shape, stands 91 cm high, and has a vane that keeps the tripod oriented into the flow. It is equipped with an Optical Backscatterance Sensor (OBS), a Marsh McBirney electromagnetic current meter, a KVH Industries Model ROV103 fluxgate digital compass, a set of four pumps that operate by an electronic timer for water/suspended sediment samples and an Ocean Sensors CTD that also serves as the data logger for the other instruments mounted on the tripod. The current meter, OBS, and pump nozzle were mounted 20 cm above the bed, and the CTD was 31 cm above the bed. The pump sampling system provided an in situ calibration for the OBS. Three samples were obtained from each cast thus providing a range of SSCs and particle sizes.

## 3. Results

The study was conducted after a peak in river discharge of  $300 \text{ m}^3 \text{ s}^{-1}$  at the end of February. Following the peak, discharge decreased steadily throughout the study period to a level of about  $50 \text{ m}^3 \text{ s}^{-1}$  around 20 March

1997 with only a minor increase evident near the end of March. Discharge dropped steadily throughout April.

Two complete spring–neap tidal cycles were observed over the course of the experiment. The tidal ranges for the first neap and spring period (31 March and 7 April) were 1.9 and 3.0 m, respectively. The ranges for the second fortnightly pair (14 and 23 April) were 1.6 and 2.4 m, respectively.

Data from the moorings were divided into subtidal and tidal sets. A description of events at tidal frequencies is based on the raw data. Subtidal sets were created from the raw data using a 40-h low-pass filter.

### 3.1. Circulation

#### 3.1.1. Subtidal currents

Significant subtidal fortnightly fluctuations occurred in landward flow near the bottom (Fig. 3). Fluctuations in near-bottom axial currents (1 mab) at Sites E and W and the near-bottom current at C1 were well correlated over most of the record (Fig. 3a). There were two neap–spring cycles over the mooring period. During the first neap tide (31 March), near-bottom axial flow was upstream and flow higher over the bottom was downstream (Fig. 3a). Similar conditions occurred around neap tide on 15 April. As the spring tide approached (7–8 April, 22–23 April), upstream bottom flow became weak at the west site and changed to downstream at the middle and east sites.

Cross-channel currents also followed a neap–spring tide pattern (Fig. 3b). During neap, currents were weak, but as spring conditions evolved, cross-channel currents near the bottom flowed from the outside to the inside of the curving channel. The strength of this flow increased from Sites E to W, i.e. as the along channel flow traversed the curving bend. Except during neap tide, flow at 6.7 mab was to the outside of the bend, indicating the role of centrifugal force in driving secondary circulation in the curving channel.

#### 3.1.2. Tidal currents

Currents measured at the anchor station varied between  $\pm 100 \text{ cm s}^{-1}$  during spring tide and  $\pm 60 \text{ cm s}^{-1}$  during neap (Fig. 4). There were subsurface flood maxima between 4 and 6 mab and surface maxima in ebb. These maxima can occur through straining of the cross-channel density field by lateral velocity shear (Turrell, Brown, & Simpson, 1996). Flood and ebb currents achieved maxima with 1.5–2 h after slack, indicating a relatively high degree of asymmetry that is typical throughout many shallow mesotidal estuaries like the Satilla (Blanton et al., 1999; Blanton, Lin, & Elston, 2002).

Axial current profiles reveal nearly uniform shear over depth for ebb currents whereas during flood, the current is strongly sheared near the bed and weakly

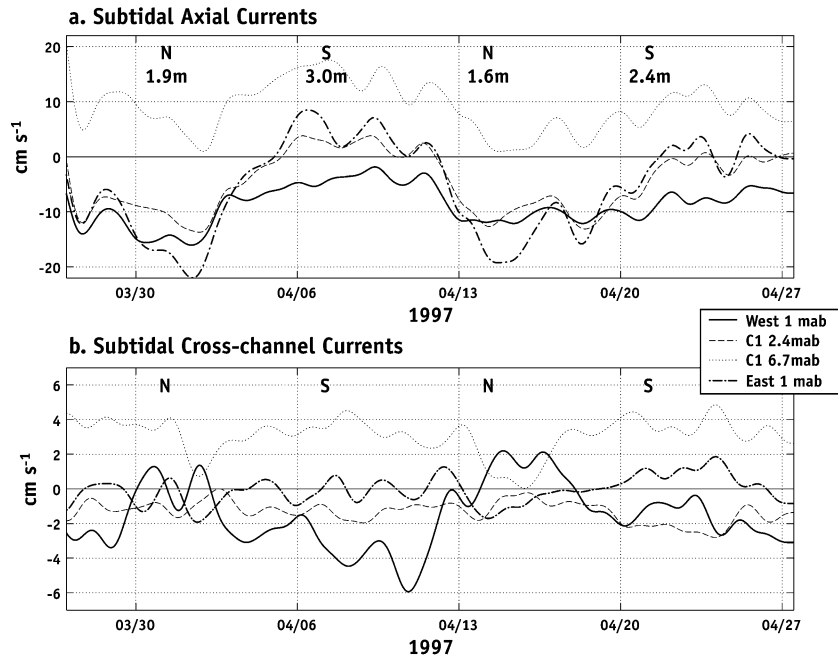


Fig. 3. Subtidal axial and cross-channel currents.

sheared higher in the water column (Fig. 4). Highest vertical shear occurred within 2 m of the bottom during flood at spring tide. Flood shear was greater than ebb shear by a factor of 2, indicating a pronounced influence of gravitational circulation on the tidal current signature (Jay & Smith, 1990).

Tidally averaged vertical current profiles were obtained by averaging the ADCP data for the two spring tides and the two neap tides observed in this study (Fig. 5). Averages were produced for each depth bin. This means that less data are included in the averages of the bins in proportion to their distance above mean low

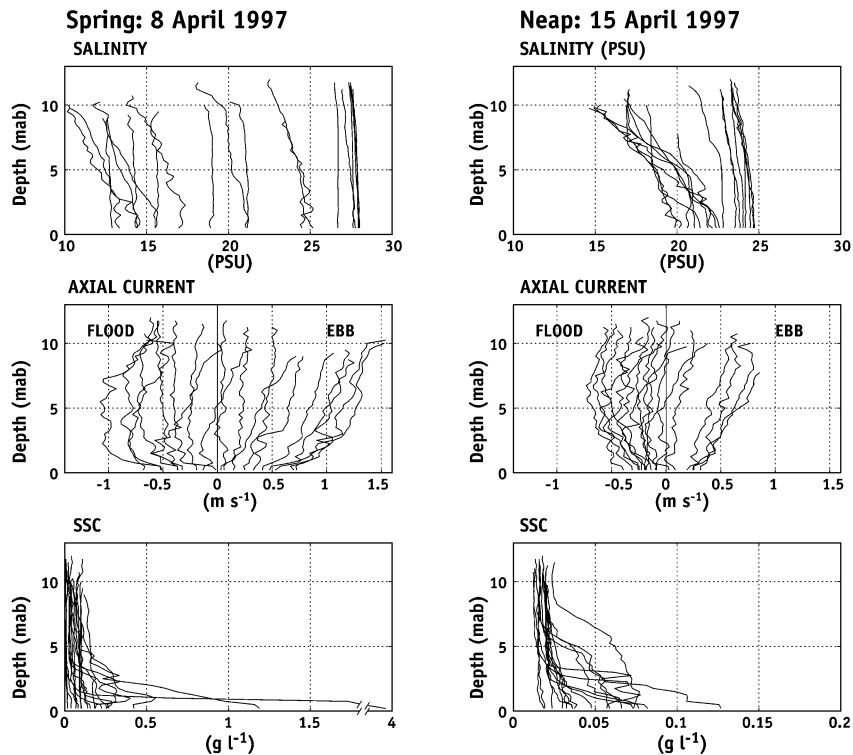


Fig. 4. Salinity, velocity, and OBS profiles.

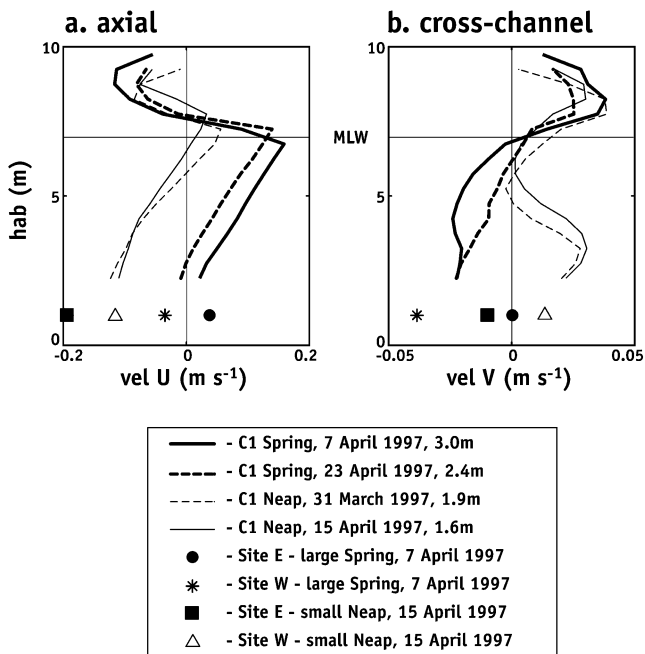


Fig. 5. Average current profile combined from ADCP and S-4 data.

water (MLW). Averages of the S-4 data from Sites E and W are superposed. The spring-tide profiles for the axial current (Fig. 5(a)) show export below MLW and import above the intertidal zone. The change to landward flow in the intertidal zone is consistent with tidally driven residual flow (Ianniello, 1977). We refer to this tidally driven landward flow as ‘tidal pumping’. Neap tide profiles, on the other hand, show import at depth (consistent with gravitational circulation) and export from the middle of the water column to MLW. Bottom currents at Site E varied greatly between neap and spring tide, showing import during neap and export during spring. The differences at Site W were more subtle—strong import at neap and weaker import at spring.

The cross-channel flow structure (Fig. 5(b)) is remarkably different between spring and neap tide. There is always strong outward flow in the intertidal zone (above MLW), but the data suggest the presence of a single cell (outward flow near surface, inward flow near bottom) during spring tide. During neap, on the other hand, there is a more complicated structure that is difficult to interpret. The data are consistent with the presence of two cells of cross-channel circulation, stacked one on top of the other. However, our observations are inadequate to verify this. The bottom cross-channel flow at Site W suggests that the secondary circulation cell is particularly well developed (strong inflow toward the center of curvature) but poorly developed (no inflow) at Site E where the channel has less curvature (Fig. 2).

In summary, we observed a spring–neap variation in the tidally averaged vertical current structure. At neap tide the structure was classic gravitational circulation,

but at spring tide the landward near-bottom flow was severely diminished and even reversed. We infer that the increased tidal range is associated with stronger tidal residual flow. Previous work (Ianniello, 1977, 1979; Li & O’Donnell, 1997; Li, Valle-Levinson, Wong, & Lwiza, 1998) suggests the structure of the residual flow is roughly the opposite phase (i.e. negates) of the gravitational circulation. Our analyses indicate that enhanced landward transport occurs at spring tides in the intertidal zone.

### 3.2. Salt flux

#### 3.2.1. Subtidal flux

Axial surveys over the course of the study showed a gradual shift landward of the salinity field (Fig. 6). At 20 km from the ocean, salinity increased from 6 to 20 PSU. At 10 km from the ocean, salinity increased from 16 to 28 PSU. Thus, the salinity throughout this part of the estuary increased and the low-salinity isohalines moved landward.

The salinity at Sites E and W confirms the shift landward of the salinity field (Fig. 7a). Salinity increased gradually from about 12 to 24 PSU at ‘W’ and from about 16 to 26 PSU at ‘E’ over a period of about 30 days. This represents a decrease in the along-channel salinity gradient from 2 to 1 PSU/km over this period.

There were wave-like salinity fluctuations superimposed on the trend of increasing salinity. The fluctuations were tightly correlated at the east and west sites and were accompanied by corresponding shifts in water level (Fig. 7b). Subtidal water-level fluctuations in estuaries can be driven by Ekman fluxes on the adjacent continental shelf (Klinck, O’Brien, & Svendsen, 1981; Wong & Moses-Hall, 1998) and by remotely forced shelf waves (Schwing, Oey, & Blanton, 1988). Episodes of depressed water level (e.g. 30 March, 14 April) were accompanied by depressions in salinity representing a seaward shift of the salinity field. The opposite was true for episodes when water level rose (e.g. 3 April, 10 April, 16 April). Thus, subtidal salinity fluctuations were positively associated with subtidal sea level fluctuations and suggest axial translations of the salinity field up and down the estuary. Fluctuations in the along-channel salinity gradient (parameterized by subtracting the two signals in Fig. 7a) are negatively correlated with similar fluctuations in water level. This finding is consistent with the advection of a *spatially varying* along-channel salinity gradient through the study area (Wong, 1995).

#### 3.2.2. Tidal fluxes

Salinity at the anchor station varied over the tidal cycle by 16 PSU at spring and by 6 PSU during neap (Fig. 4a). Vertical salinity (density) difference was greater during neap, particularly during ebb. Seim, Blanton, and Gross (2002) showed that stratification in

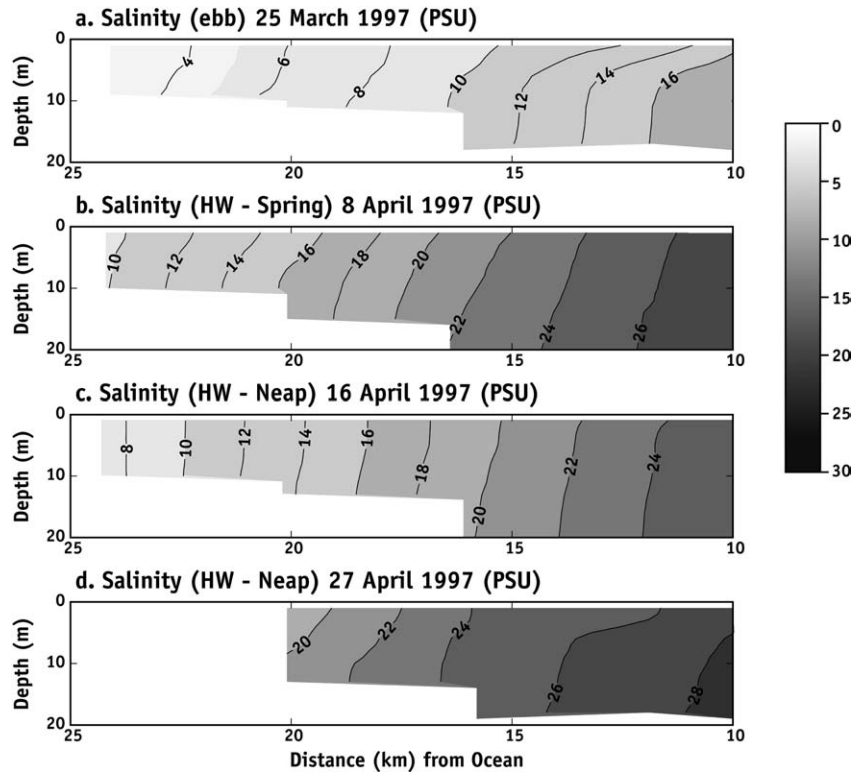


Fig. 6. Axial salinity distribution.

the lower 2.5 m was established first at Site ‘W’ about an hour after low water slack (LWS) and at the anchor station about an hour later. Given an along-channel separation of 1.5 km, the stratified fluid appeared to travel at a rate of about  $35 \text{ cm s}^{-1}$ , typical of the flows observed at that stage of the tide. The malfunction of the bottom salinity sensor at Site E prevented us from following the onset and propagation of stratified fluid through the study area.

### 3.3. Sediment flux

#### 3.3.1. Fortnightly cycles in sediment mobilization

Sediment profiles during neap and spring revealed pronounced vertical stratification in SSC during parts of the tidal cycle (Fig. 4c). The highly turbid layers near the bottom occurred around LWS and during the early stages of flood and were found within the lowest 2 m, coincident with the zone of maximum shear. Maximum concentrations near bottom were greater by an order of magnitude during spring tide. Similar profiles with even larger near-bottom SSCs were observed landward of Bailey Cut in a previous study (Blanton et al., 1999).

Acoustic backscatter data from the ADCP can be interpreted as an uncalibrated source of suspended sediment information. A comparison of echo intensity and axial currents (Fig. 8) showed expected differences during spring versus neap tide. The overall levels of both parameters were significantly higher during spring tide. The largest echo intensity occurred near bottom, also most obvious in the spring tide example. During both spring and neap, echo intensity reached higher in the water column during the flood phase. Intensity dropped to minimum levels at high water, indicating a relative clearing of the water column. Backscatterance at low water was slightly higher than at high water.

A comparison of uncalibrated OBS data with bottom pressure (Fig. 9) at Sites ‘E’ and ‘W’ showed substantial

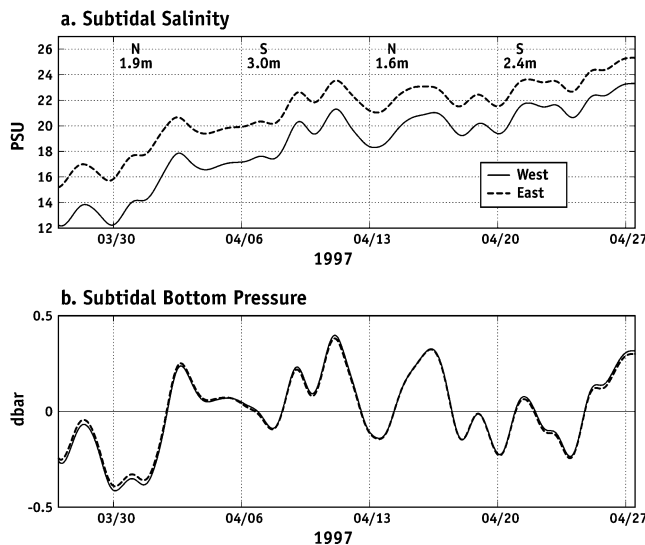


Fig. 7. Subtidal salinity and SSP fluctuations.

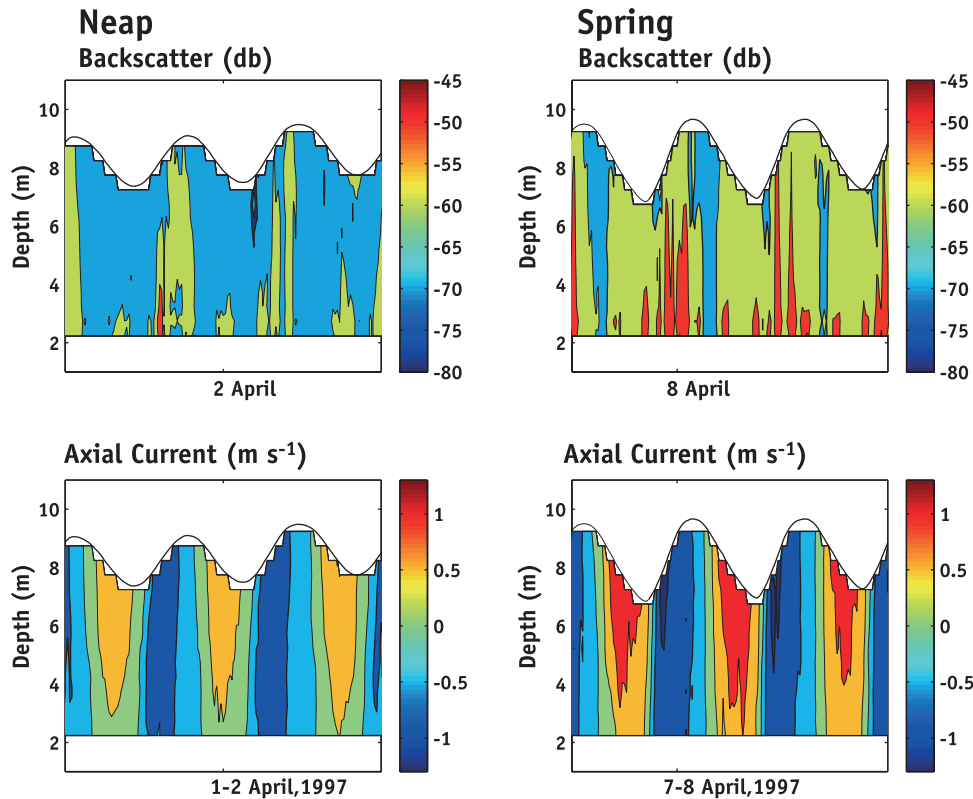


Fig. 8. ADCP current and echo intensity profiles.

spatial heterogeneity in the study reach. OBS values at both sites diminished to background levels at high and low water. The onset of relatively high OBS at neap occurred at mid-flood stage at 'E' and at later flood stages at 'W'. Mid-water levels at both sites were essentially at background.

During spring tide, OBS values were noticeably higher at both sites. Near-bottom values were 50% higher at 'W'. Mid-water values in the east were as high, if not higher, than near-bottom values during flood and near the end of ebb. High bottom and mid-water values occurred near the time of low water and into the early stages of flood. The most significant difference occurs in the higher OBS values at 'W' throughout the rising tide, clearly indicating spatial heterogeneity of the suspended sediment fields (Fig. 9).

### 3.3.2. Along-channel variations in salt and sediment fluxes

Spatial heterogeneity is further emphasized by multiplying salinity and OBS data by the axial component of bottom velocity and accumulating the products as a progressive flux diagram (Fig. 10). We used the near-bottom axial velocity ( $\text{m s}^{-1}$ ) multiplied by salinity ( $\text{kg m}^{-3}$ ) to yield the salt flux ( $\text{kg m}^{-2}$ ). For sediment flux, we assumed that 1 unit of OBS output equaled  $10^{-3} \text{ kg m}^{-3}$ , which when multiplied by velocity gave

sediment flux ( $\text{kg m}^{-2}$ ). The prevailing negative increase in cumulative fluxes indicates a net landward flux of salt and sediment along the bottom. The spring–neap differences in tidal ranges have a clear effect on the bottom flux of salt and sediment.

Cumulative salt fluxes at Sites 'E' and 'W' (Fig. 10(a)) were similar throughout the first two-thirds of the first fortnightly cycle (26 March to 5 April), suggesting that the study area was neither accumulating nor getting rid of a significant amount of salt along the bottom. During the last one-third approaching the large spring tide, the cumulative flux at 'W' decreased slightly, but cumulative flux at 'E' began to increase until 13 April. This suggests that near-bottom salt content decreased. From spring to the next neap tide, the curves are approximately parallel only to diverge once again as the next spring tide approached. Note that the diverging pattern is primarily a function of the flow, since the salinity difference between the two sites was no more than 2–4 PSU throughout the study period (Fig. 7).

Cumulative sediment fluxes at the two sites (Fig. 10(b)) indicate a net landward flux of suspended sediment throughout the first 20 days after which the OBS sensors became fouled. Throughout the period, there was more bottom flux during flood than during ebb, particularly at Site 'W', substantiating the higher bottom stress during flood as described earlier. From 27 March through neap and as spring tide approached, net flux

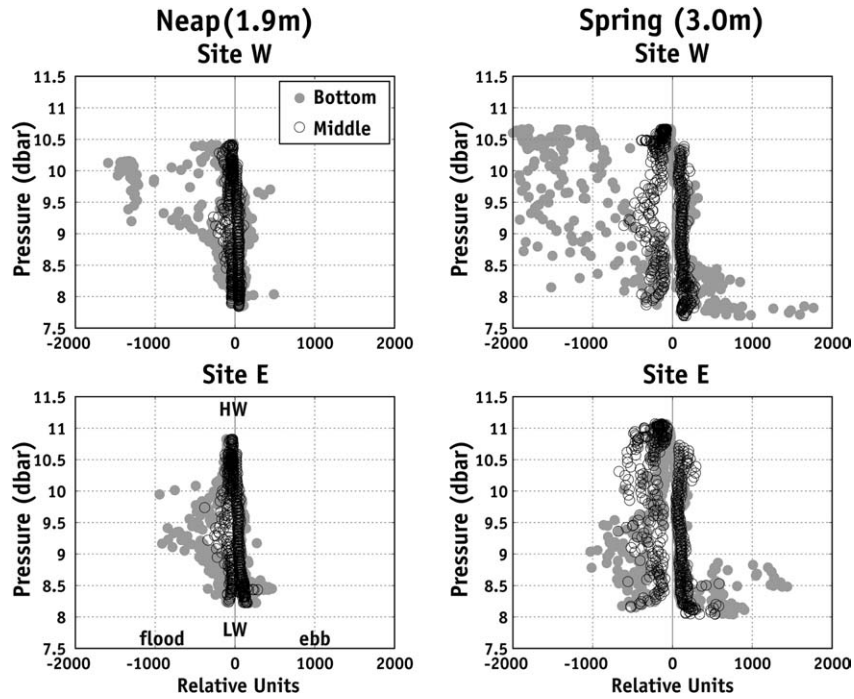


Fig. 9. OBS versus pressure at sites E and W.

was about the same until the first spring tide when flux at ‘W’ increased suddenly during flood tide. A weak accumulation of suspended sediments at the bottom over that period is indicated by the slightly different

slopes of the two curves. Since a similar increase was absent at ‘E’, suspended sediments were apparently evacuated from the near-bottom zone along the thalweg somewhere between the two sites.

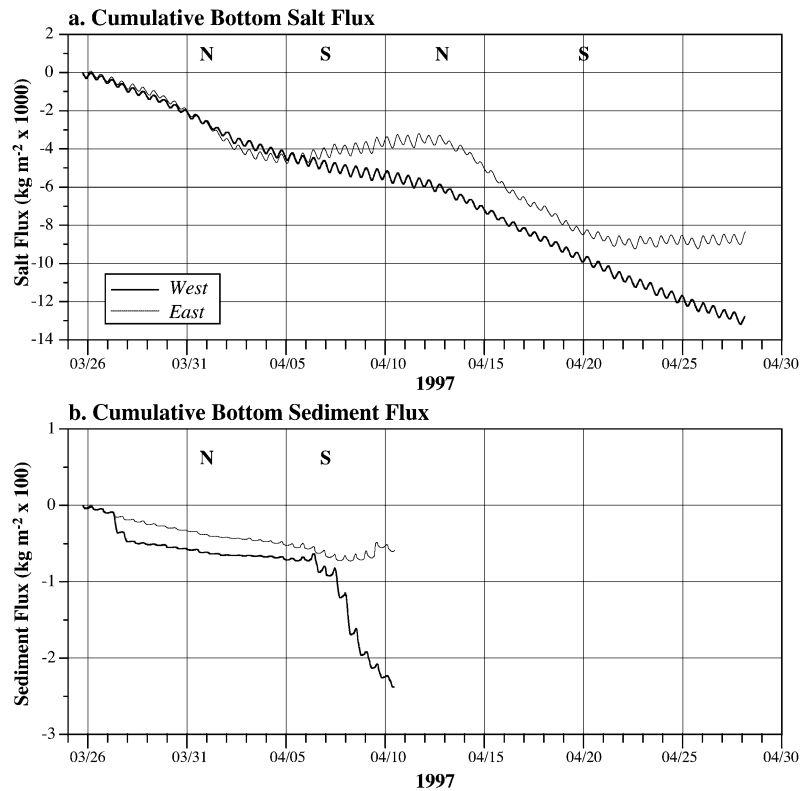


Fig. 10. Salt and sediment fluxes at east and west sites.

The lack of consistency between the landward and seaward ends of the curving channel, despite both moorings lying only a short distance, further emphasizes the spatial heterogeneity of the flow regime. The salt flux difference (Fig. 10(a)) implies a divergence of salt flux along the bottom in this reach of the estuary during spring tide, perhaps indicating a loss to higher levels of the water column and/or laterally. A similar divergence was noted in the sediment flux (Fig. 10(b)), partially as a result of sediment re-suspension to higher levels of the water column. The strong cumulative negative sediment fluxes at 'W' remained active more than 2 days after spring tide.

In summary, sediment flux was strongest during flood and the net flux was landward as a result. Spring-tide currents appear to exceed the threshold for re-suspension as evidenced by the observed large increase in SSCs. The sediment flux diverged along the channel bend during spring tide. Even though there appeared to be a net landward flux, the flux strength was very heterogeneous over the reach sampled.

## 4. Discussion

### 4.1. Fortnightly flow regimes

The strong divergence of bottom salt flux observed at spring tide is consistent with a transfer of salt to the intertidal zone, both laterally and vertically. The amount of salt lost upward depends on the size of a horizontal plane that changes with the fluctuations in size of the intertidal area. This forces us to make too many assumptions on the size of the control volume that receives this salt and prevents us from making a meaningful estimate of the fortnightly cycle of salt content that results from such a divergence. There is no obvious fortnightly signal in the mooring bottom salinity data, thus a spatially consistent salt flux must be maintained. A test on whether or not the salt flux varies with the neap–spring cycle would require monitoring the salt inventory along a substantial length of the estuary.

The weaker mixing at neap tide allows a clear gravitational mode to occur, as shown by the ADCP data with seaward flow above the middle of the water column and landward flow below. As spring tide approaches, an increase in strength of tidal pumping drives mass landward on the shallow flanks, which requires seaward flow in the deep channel to balance the mass (Li & O'Donnell, 1997; Li et al., 1998). It would appear that the increased tidal flux at spring tide was sufficient to completely shut down the landward flow usually attributed to the gravitational mode at the bottom at the seaward and middle portion of the study domain.

The bottom salt flux measurements (Fig. 10(a)) offer clues about several estuarine dynamic processes. The

way the flux has been calculated includes fluxes by subtidal gravitational flow and tidal pumping. First, the decrease in upstream flux during spring tides coupled with its coincident increase in the intertidal zone (Fig. 5) implicates tidal pumping as playing an important role in maintaining the upstream salt flux during spring tide. This means that the salt flux is carried higher in the water column on spring tide. Furthermore, tidal pumping should become less effective when stratification is strong (i.e. when river flow is high and/or surface salinity is lower).

There are other important circulation features that change during a fortnight. During the approach of the spring tide of 8 April (Fig. 3), bottom flow toward the inside of the bend decreased from a minimum at Site 'E', where channel curvature is a minimum, to an intermediate value at Site 'C1' to a maximum at Site 'W'. The situation at neap tide is much more confusing.

The spatial change in secondary circulation has an effect on the along-channel flow. Seim et al. (2002) analyzed and compared axial and cross-axial currents at Sites 'E' and 'W' (Fig. 2). Axial ebb currents at 'E' were generally weaker and briefer than those at 'W' over the spring–neap cycle. However, during spring, flood currents were consistently stronger at 'W' while ebb currents were consistently stronger at 'E' (see Figs. 4 and 5 in Seim et al. (2002)). In other words, the axial current increased its strength in the *downstream* direction during spring tides, a condition attributed to the addition of momentum to bottom currents by the cross-axis secondary circulation acting throughout the channel bend (Seim & Gregg, 1997). At neap, secondary circulation is too weak to penetrate the stratification near the bottom. Therefore, strong flood currents at spring tide would cause bottom stress to increase in the landward direction along the channel bend, and thereby account for the significantly higher OBS values at 'W' observed during spring tide (Fig. 9).

### 4.2. Sediment movement upstream

A study by Seim et al. (2002) showed that Reynolds stresses at Site C2 (Fig. 2) varied by a factor of four during ebb tide and increased steadily as spring tide approached. Moreover, salinity data at the site (not shown) indicated that near-bottom stratification present at ebb was absent during flood. This raised the gradient Richardson number well above 0.25 over most of the ebb phase and lowered the shear stress at the bottom (Seim et al., 2002). As a result, the flood stage usually had higher stress and higher velocity shear at the bottom than the ebb (Fig. 4), which provided a regime with preferential sediment transport landward.

Estimates of the drag coefficient ( $C_d$ ) gave an average  $C_d$  value of 0.0017, but there is considerable scatter in the relationship between Reynolds stress and the mean

flow, the squared correlation being 0.7 (Seim et al., 2002). Many of the highest stress estimates during spring tides were not well represented by this regression. This was attributed to the fact that as flow conditions approached spring tide, near-bottom stratification produced on ebb begins to break down (see subsequently). The value of  $C_d$  for the spring-tide part of the record was 0.0025. The higher drag coefficient coupled with higher velocities generates significantly higher bottom stress at spring tide.

The tidally averaged currents near bottom (Figs. 3 and 5) show significant differences between the seaward and landward sites and between spring and neap. At the east site, spring tide currents are  $5 \text{ cm s}^{-1}$  export versus  $20 \text{ cm s}^{-1}$  import at neap. At the west site, there is a modulation in the strength of landward flow. In all regards, the overall tendency was for a net landward transport.

The temporal and vertical structures of acoustic backscatter (Fig. 8) are quite similar to the observations in the Weser estuary (Dyer, 1994). The small zones of high concentration seen at the bottom of the Weser and the Satilla may be interpreted as local erosion from the bed. The eroded sediment is entrained upward into the flow and joins other sediment that was re-suspended off the bed farther upstream.

The bottom stress regime sets the scene for sediment movement. Bottom stress estimates at Site C indicated a larger drag coefficient during spring tide (Seim et al., 2002). The Richardson number ( $R_i$ ) was significantly greater during neap tide and was correlated with smaller Reynolds stress at the bottom. Large/small  $R_i$  during neap/spring tide was thought to be due, in part, to variations in stratification within the bottom boundary layer. There was the expected fortnightly variability in bottom stress, but there was a pronounced difference between flood versus ebb no matter what the neap-spring phase.

Maximum values of bottom stress reached  $10 \text{ cm}^2 \text{ s}^{-2}$  on each flood tide but were less than  $5 \text{ cm}^2 \text{ s}^{-2}$  on ebb. Since the fastest flood and ebb currents occurred a short time after slack water, bottom stress was significantly greater in the early stages of flood compared with those during ebb. This is supported by medium levels of echo intensity that, in general, extend closer to the surface during flood than during ebb (Fig. 8).

Subtidal variations in bottom salt flux suggest that tidal pumping plays a more important role in upstream salt transport at spring tide, which in turn implies that near-bottom velocities are not strongly landward at that time (Fig. 3). However, tidal pumping cannot be as effective for sediments as for salt since sediments are not mixed as effectively upward into the water column. Landward sediment transport appears to be associated with preferred re-suspension during flood tides, despite seaward mean velocities (C.T. Friedrichs, personal com-

munication). Similar dynamics were observed at the landward end of the bend, but at the seaward end, sediment transport on ebb and flood was roughly equal and there was no clear net transport direction.

There appeared to be a resistance to mobilization during the build-up to the strong spring tide of 7 April (Fig. 10(b)). Just 1 day before maximum stress, large quantities of bed sediments were suddenly eroded and continued to be eroded at a slowly decreasing rate (indicated by the slow decrease of cumulative sediment flux) until 11 April, 4 days after spring tide. Higher concentrations of suspended sediments were also observed in the Weser for decreasing tidal ranges from spring to neap (Grabemann & Krause, 2001). They concluded that consolidation of sediments during the previous neap provided a resistance to erosion up to the time just before the maximum bottom stress at spring tide. Our data are consistent with this as well.

Due to its heterogeneous distribution of sediment types as well as the multiple lateral sources of sediments from the many tidal creeks, the Satilla is likely to have multiple estuarine turbidity maxima (ETMs) tied to multiple sedimentary compartments of the estuary (see Section 1). Data (not shown) suggest that the position of multiple highly turbid zones is related to discharge. The response of turbid zones to river discharge has been reported in other estuarine systems (Allen et al., 1980; Fettweis, Sas, & Monbaliu, 1998; Gelfenbaum, 1983; Uncles et al., 1998). During April 1995, discharge was about  $120 \text{ m}^3 \text{ s}^{-1}$  and maximum turbidity was found around 13 km from the ocean (Blanton et al., 1999). By contrast, a similar section in July 1996, when discharge was below  $20 \text{ m}^3 \text{ s}^{-1}$  showed maximum turbidity located farther upstream in three separate 'compartments'.

#### 4.3. Tidally averaged flow in the channel bend

We use a cartoon to visualize fortnightly variations of the residual circulation in a channel bend (Fig. 11). The near-bottom and mid-water column flow is based on observations along the thalweg (Fig. 3). Currents at the middle and west site were measured where the channel had the most curvature while those at the east site were measured where the channel curvature was smaller. We infer the other circulation features based on a conservation of volume transport in any given cross-section.

Secondary circulation in a channel bend interacts with gravitational circulation and tidal pumping. Secondary circulation acting throughout channel bends can overturn the water column as it travels around the bend (Seim & Gregg, 1997). During flood, the cross-axis bottom current adds momentum to the bottom current in the landward direction, while the ebb current adds momentum to the bottom current in the seaward direction. Secondary circulation at neap tide is too weak to

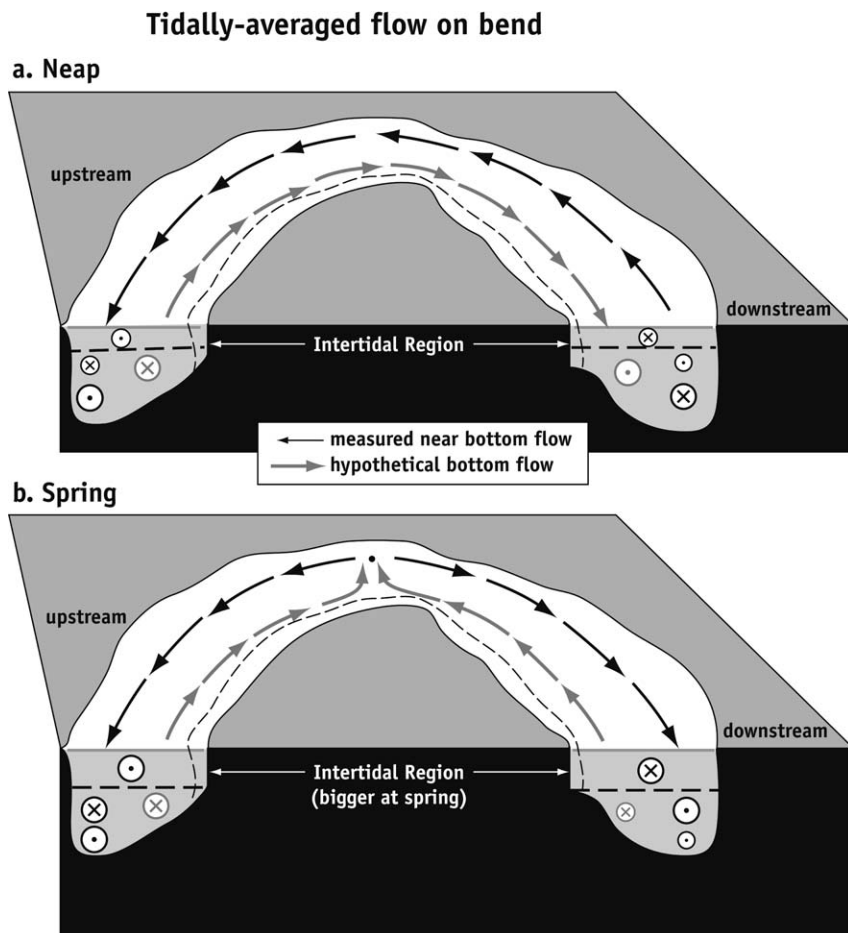


Fig. 11. Tidally averaged flow on a channel bend.

penetrate the stratification near the channel bottom and interferes with the gravitational circulation mode. A well-developed gravitational mode at neap is illustrated by relatively strong bottom landward flow going through the deep part of the channel (Fig. 11). This flow decreases in strength with distance from bottom and changes to seaward at the top of the intertidal zone. Within the intertidal zone, the flow is weakly landward due to tidal pumping. In order to achieve a neap-tide balance in a given cross-section, we infer a relatively strong seaward flow in shallow areas below MLW to compensate for the predominantly landward flow over the deep channel.

There is a significant change in the bottom flow regime over the fortnightly cycle. At neap tide, bottom flow is landward throughout the channel bend (Fig. 3). At spring tide when tidal pumping is maximized, strong landward flow exists in the intertidal zone (Fig. 5). Strong tidal pumping generally produces a seaward bottom flow in the deeper parts of the channel (Li & O'Donnell, 1997) that, in our case, extends to mid-water levels. However, in the bend, the subtidal bottom flow changes direction from floodward at the landward end to ebbward at the seaward end. This strongly suggests

that the secondary circulation gradually weakens and eventually reverses the seaward flow due to tidal pumping at the landward end of the bend. As a result, bottom stress from flood currents are enhanced by the subtidal flow at spring tide producing a seaward to landward increase in bottom stress and accounts for significantly higher OBS values observed during spring tide at the landward end of the channel bend (Fig. 9 (upper right)).

Assuming our inferences are qualitatively correct, the neap near-bottom landward flow in the thalweg is more or less continuous throughout the axial extent of the channel and implies the presence of a seaward flow below MLW in the shallow areas. The spring-tide residual flow, however, has a gyre-like pattern (Fig. 11). The seaward flow in the straight part of the thalweg is replaced by landward flow in the bending thalweg. We speculate that the switch-over occurs somewhere in the maximum curvature of the bend. To close this flow pattern, the bottom flow along the thalweg changes to seaward flow in the shallow areas thereby producing a cyclonic gyre landward of the 'switch-over point' and seaward downstream of the point.

## 5. Conclusions

This study has revealed that the salt and sediment flux in a curved estuarine channel results from a superposition of effects occurring at two scales. First, at scales larger than the channel bend, there is a neap–spring cycle in exchange flow. At neap, there is classical gravitational circulation. At spring, the exchange flow can be reversed by strong tidal pumping. In general, near-bottom landward flow is reduced, even reversed, at spring tides, but indications are that the landward flux of salt and sediment persists at the large scale.

Second, at the smaller scales of channel bends, secondary circulation drives tidally averaged divergent flow near the bed due to along-channel variations in its strength. The strength of the circulation is related to tidal range (through the flow speed) and this temporal variability can be reinforced by variations in vertical stratification. The higher stratification associated with neap tide suppresses secondary circulation, and we tend to have weak secondary circulation at neap. Secondary circulation becomes much stronger during spring tides.

For the landward fluxes of sediment and salt to persist in the presence of strong tidal pumping (spring tides), they must be carried higher in the water column and/or laterally over the shoals. In our study, the magnitude of the salt gradient showed no evidence of a neap–spring tide modulation (Fig. 7), which would suggest a similar modulation in flux. Our data do not extend over a sufficient length of the estuary to definitely ascertain if there is a fortnightly modulation of the total salt content of the estuary. But the evidence presented here illustrates that the landward transport of salt in the intertidal zone during spring tide must play a role. Landward pumping of mass increases in the intertidal zone (Li & O'Donnell, 1997) and there is a compensating seaward flow in the deep channels (Fig. 3) that would suggest the seaward removal of salt along the bottom. However, strong tidal pumping at spring tide could compensate for this by moving salt landward even as it is advected seaward along the bottom upward into the intertidal zone thus maintaining the landward flux of salt.

Sediment flux is generally upstream, associated with the preferential suspension on flood and the gravitational circulation. However, the divergent near-bottom flow on the bends disrupts this upstream flow, leading to sediment flux divergence (causing channel deepening) in the middle of the bends and sediment flux convergence (causing shoaling) between bends. In the presence of several sedimentary compartments, this would explain the lack of a single clear ETM in the Satilla River and is consistent with the existing topography associated with each compartment (deep holes on bends separated by shoals between bends).

The pronounced fortnightly sensitivity of stress and stratification during the flood or ebb phase of the tide is

likely to have a large impact on the net flux of salt and sediment as well as be important in long-term budgets of the estuary. Several important questions are raised by this study. Does the total salt content of the estuary vary fortnightly over a reach encompassing many channel bends? How does the lateral and vertical structures in the axial flux of salt and sediments vary over the neap–spring cycle?

These questions can only be resolved with observations of currents, salinity, and suspended sediments that extend laterally into the intertidal zone and throughout much of the axial extent of the estuary. This requires small fast-response current meters, pressure gages and salinometers that can be deployed within the intertidal zone. Use of a high-resolution numerical model capable of handling the wetting and drying of spatially large intertidal areas would aid in resolving the complex issues raised here.

## Acknowledgements

We wish to thank several people who made indispensable contributions to this study. Tom Gross provided critical assistance in the preparation and deployment of BASS. Francisco Andrade, Anna Barbosa, and Adriano Bordelo analyzed much of the field data described in this article. Their participation was made possible by a grant from the Fundação Luso-Americana para Desenvolvimento (FLAD). We are grateful to Dr Charles Buchanan (FLAD) for his enthusiastic support.

The able crew (Captain Jay Fripp, Raymond Sweatte and Mike Richter) of the R/V BLUE FIN of the Skidaway Institute of Oceanography gave us dedicated enthusiasm and support in carrying out the field experiments.

We gratefully acknowledge the following agencies who supported the work described in this article: the Georgia Coastal Zone Management Program (Grant No. RR100-279/9262764), National Science Foundation (LMER Grant No. DEB-9412089 and LTER Grant No. OCE-9982133), Georgia Sea Grant Program (Grant No. R/EA-15), NOAA Coastal Ocean Program (Grant to South Carolina SeaGrant Consortium entitled 'Tidal Circulation and Salt Transport in a Tidal Creek-Salt Marsh Complex'), Junta Nacional de Investigação Científica e Tecnológica, Project 87-349 and a grant to the senior author from the W.J. Fulbright Commission through Comissão Cultural Luso-Americana.

## References

- Allen, G., Salomon, J., Bassoulet, P., Penhout, Y. D., & DeGranpre, C. (1980). Effects of tides on mixing and suspended sediment transport in macrotidal estuaries. *Sedimentary Geology* 26, 69–80.
- Blanton, J., Alexander, C., Alber, M., & Kineke, G. (1999). The mobilization and deposition of mud deposits in a coastal plain estuary. *Limnologia* 29, 293–300.

- Blanton, J., Lin, G., & Elston, S. (2002). Tidal current asymmetry in shallow estuaries and tidal creeks. *Continental Shelf Research* 22, 1731–1743.
- Dyer, K. (1994). Estuarine sediment transport and deposition. In K. Pye (Ed.), *Sediment transport and depositional processes* (pp. 193–218). Oxford: Blackwell Scientific.
- Dyer, K. (1997). *Estuaries: A physical introduction* (2nd ed.). Chichester: Wiley.
- Fettweis, M., Sas, M., & Monbaliu, J. (1998). Seasonal, neap–spring and tidal variation of cohesive sediment concentration in the Scheldt Estuary, Belgium. *Estuarine, Coastal and Shelf Science* 47, 21–36.
- Gelfenbaum, G. (1983). Suspended-sediment response to semidiurnal and fortnightly tidal variations in a mesotidal estuary: Columbia River, USA. *Marine Geology* 52, 39–57.
- Geyer, W., Woodruff, J., & Traykovski, P. (2001). Sediment transport and trapping in the Hudson River. *Estuaries* 24, 670–679.
- Grabemann, I., & Krause, G. (2001). On different time scales of suspended matter dynamics in the Weser estuary. *Estuaries* 24, 688–698.
- Ianniello, J. P. (1977). Tidally induced residual currents in estuaries of constant breadth and depth. *Journal of Marine Research* 35, 755–786.
- Ianniello, J. P. (1979). Tidally induced residual currents in estuaries of variable breadth and depth. *Journal of Physical Oceanography* 9, 962–974.
- Jay, D., & Smith, J. (1990). Residual circulation in shallow estuaries, 2: weakly stratified and partially mixed, narrow estuaries. *Journal of Geophysical Research* 95, 733–748.
- Klinck, J., O'Brien, J., & Svendsen, H. (1981). A simple model of fjord and coastal circulation interaction. *Journal of Physical Oceanography* 11, 1612–1626.
- Li, C., & O'Donnell, J. (1997). Tidally driven residual circulation in shallow estuaries with lateral variation. *Journal of Geophysical Research* 102, 27915–27929.
- Li, C., Valle-Levinson, A., Wong, K. C., & Lwiza, K. M. (1998). Separating baroclinic flow from tidally induced flow in estuaries. *Journal of Geophysical Research* 103, 10405–10417.
- Oertel, G., & Dunstan, W. (1981). Suspended-sediment distribution and certain aspects of phytoplankton production off Georgia, USA. *Marine Geology* 40, 171–197.
- Postma, H. (1961). Transport and accumulation of suspended matter in the Dutch Wadden Sea. *Netherlands Journal of Sea Research* 1, 148–190.
- Schwing, F., Oey, L.-Y., & Blanton, J. (1988). Evidence for non-local forcing along the southeastern United States during a transitional wind regime. *Journal of Geophysical Research* 93, 8221–8228.
- Seim, H., Blanton, J., & Gross, T. (2002). Direct stress measurements in a shallow sinuous estuary. *Continental Shelf Research* 22, 1565–1578.
- Seim, H., & Gregg, M. (1997). The importance of aspiration and channel curvature in producing strong vertical mixing over a sill. *Journal of Geophysical Research* 102, 3451–3472.
- Sternberg, R., Kineke, G., & Johnson, R. (1991). An instrument system for profiling suspended sediment, fluid, and flow conditions in shallow marine environments. *Continental Shelf Research* 11, 109–122.
- Turrell, W., Brown, J., & Simpson, J. (1996). Salt intrusion and secondary flow in a shallow, well-mixed estuary. *Estuarine, Coastal and Shelf Science* 42, 153–169.
- Uncles, R., Easton, A., Griffiths, M., Harris, C., Howland, R., King, R., Morris, A., & Plummer, D. (1998). Seasonality of the turbidity maximum in the Humber-Ouse Estuary, UK. *Marine Pollution Bulletin* 37, 206–215.
- Williams, A., Tochko, J., Keohler, R., Grant, W., Gross, T., & Dunn, C. (1987). Measurements of turbulence in the oceanic bottom boundary layer with an acoustic current meter array. *Journal of Atmospheric and Oceanic Technology* 4, 312–327.
- Wong, K. (1995). On the relationship between long-term salinity variations and river discharge in the middle reach of the Delaware Estuary. *Journal of Geophysical Research* 100, 20705–20713.
- Wong, K., & Moses-Hall, J. (1998). On the relative importance of remote and local wind effects to the subtidal variability in a coastal plain estuary. *Journal of Geophysical Research* 103, 18393–18404.